J. Membrane Biol. 144, 231–244 (1995)

The Journal of
Membrane
Biology

Tracking Movements of Lipids and Thy1 Molecules in the Plasmalemma of Living Fibroblasts by Fluorescence Video Microscopy with Nanometer Scale Precision

B.W. Hicks[1], **K.J. Angelides**[1,2]

[1]Department of Cell Biology, Baylor College of Medicine, Houston, TX 77030
[2]Division of Neuroscience, Baylor College of Medicine, Houston, TX 77030

Received: 15 July 1994/Revised: 9 December 1994

Abstract. The lateral diffusion of 100 nm fluorescent latex microspheres (FS) bound to either *N*-biotinyl-phosphatidyl-ethanolamine or the glycosylphosphatidylinositol-linked protein Thy1 were monitored in the plasmalemma of primary rat fibroblasts by single particle tracking of FS centroids from digital fluorescence micrographs. A silicon intensified target camera was found to be superior to slow scan cooled CCD and intensified interline transfer CCD cameras for monitoring lateral diffusion of rapidly moving FS with nanometer level precision. To estimate the maximum tracking precision, a 4 sec-sequence comprising 120 images of FS fixed to a cover glass was obtained. The mean distance of the centroids from the origin was 7.5 ± 0.4 nm, and no centroids were beyond 16 nm from the origin. The SIT camera was then used to track FS attached to lipids and Thy1 molecules on the surface of fibroblasts. The lateral diffusion of lipid-bound FS was unconstrained, and the ensemble averaged diffusion coefficient was 0.80×10^{-9} cm^2/sec. Thy1-bound FS existed in two mobility populations, both of which demonstrated constrained mobility. The rapidly moving population, comprising 61% of the total, had an ensemble diffusion coefficient of 6.1×10^{-10} cm^2/sec, and appeared to be restricted to domains with a mean length of about 700 nm. The slowly moving population, comprising about 39% of the total, had a diffusion coefficient of 5.7×10^{-12} cm^2/sec. These results demonstrate that nanovid can be extended to the realm of fluorescence microscopy and support previous studies indicating that while the lateral mobilities of at least some lipids are not constrained to small domains by barriers to lateral diffusion in the fibroblast plasmalemma, a peripheral membrane protein which is bound only by a lipid anchor can be prevented from diffusing freely.

Correspondence to: K.J. Angelides

Key words: Lateral diffusion — Plasma membrane — Single particle tracking — Nanovid — Fluorescence microscopy — Video microscopy

Introduction

Compartmentalization is a recurring theme in biology. The cellular plasma membrane is compartmentalized into microdomains which have compositions and functions unique from the bulk membrane (Fertuck & Salpeter, 1976; Yechiel & Edidin, 1987; Haverstick & Glaser, 1988; Black, Kocsis & Waxman, 1990; Lupa & Caldwell, 1991; Rogers & Glaser, 1991). Theoretical and empirical studies from artificial membranes predict that a cellular membrane organized into an archipelago of multiple microdomains could limit the long range lateral mobilities of components in the membrane (Rubenstein, Smith & McConnell, 1979; Owicki & McConnell, 1980; Saxton, 1987). Direct evidence for this requires the ability to probe membrane structure on a submicron scale. Nanovid, following the movements of 20–40 nm colloidal gold particles bound to specific components of the membrane by video enhanced DIC or brightfield microscopy (Allen, Allen & Travis, 1981; de Brabander et al., 1986, 1989, 1991; Geerts et al., 1987) and single particle tracking analyses (Gross & Webb, 1988; Gelles, Schnapp & Sheetz, 1988; Qian, Sheetz & Elson, 1991; Kusumi, Sako & Yamamoto, 1993; Saxton, 1993), have emerged as powerful tools to probe translational movements at the submicron level. Use of these techniques has provided insight into the mechanisms of cell motility (Sheetz et al., 1989; Kucik, Elson & Sheetz, 1990; Kucik et al., 1991; Forscher, Lin & Thompson, 1992), ATPase motor mechanics (Gelles et al., 1988; Sheetz & Kuo, 1993), and the organization of the plasma membrane and cytoskeleton (Lee et al., 1993; Schmidt et al., 1993; Sako & Kusumi, 1994).

The use of fluorescent microscopy in membrane dynamics has been largely restricted to ensemble techniques such as postelectrophoresis relaxation, fluorescence recovery after photobleaching (FRAP), and excimer formation measurements (Poo, 1981; McCloskey & Poo, 1984; Eisinger, Flores & Peterson, 1986). Limitations inherent in these techniques include the ability to monitor only the behavior of molecular ensembles, the inability to accurately determine differences between isotropic diffusion and membrane flow, and the inability to probe membrane structure on a submicron scale. Tracking individual LDL and viral receptors on the surface of fibroblasts is the sole application of fluorescence microscopy to single particle tracking (Gross & Webb, 1988). While this work was valuable in terms of its data analysis, it has limited potential because the probes could not be modified to monitor other membrane components. An alternative approach that offers several advantages is fluorescence nanovid microscopy (FNM) which can be used to study diffusion of individual membrane components by tracking modified fluorescent latex spheres (FS) with diameters ranging from 30 to 100 nm (Hicks & Angelides, 1992, 1994*a,b;* Fein et al., 1993).

To demonstrate the methodology of FNM, we monitored the lateral mobility of *N*-biotinyl-phosphatidylethanolamine (bPE) and the glycosylphosphatidylinositol (GPI) linked Thy1 antigen in the membrane of primary rat fibroblasts. Attention was focused on the area of the membrane directly above the organelle-rich regions of the cytoplasm, where conventional nanovid has limitations. Real time digitization of the video output from a silicon intensified target (SIT) camera provided records of the dynamic behavior of individual FS, and image sequences were stored in digital format. Single particle tracking (SPT) was done by determining the intensity weighted centroids of fluospheres (FS) in sequential images (Gelles, Schnapp & Sheetz, 1988; Schnapp, Gelles & Sheetz, 1988) and diffusion coefficients (D_c) were obtained from the ensemble average mean square displacements (MSD) (Qian et al., 1991). As observed by FRAP and conventional nanovid, lipid diffusion was found to be essentially unconstrained regardless of its position on the cell surface. Thy1 demonstrated two populations based on lateral mobility as seen previously by FRAP (Zhang et al., 1992), and analysis of the rapidly moving fraction suggests that it may be restricted to domains with a mean diameter of about 700 nm. That fluorescence nanovid microscopy is a practical extension of the nanovid technique is demonstrated by the ability to accurately monitor lipid and GPI-linked protein movements on living cell surfaces. Technical considerations for performing FNM and the potential advantages of this methodology over conventional nanovid are discussed.

Materials and Methods

Cell Culture

Fibroblasts were isolated from the hind limb of P2 or P3 rats. After enzymatic and mechanical dissociation, cells were plated in medium A (minimum essential media supplemented with 10% fetal bovine serum). Contaminating myoblasts were either outgrown or fused to make tubes which did not survive passage. Cells were passed three times before use and were >98% Thy1 positive when used. To minimize the effects of the extracellular matrix, only newly plated cultures were examined by SPT. Four to twelve hours before labeling the plasmalemma the cells were trypsinized and plated in chambers for the inverted microscope that consist of a 35 mm plastic culture dish with a 20 mm whole drilled out and replaced with a 25 mm collagen and poly-D-lysine coated, number 1 coverslip. The results reported are from four different fibroblasts preparations using at least four cultures from each preparation.

Preparation of Labeled Microspheres

Neutralite avidin, red carboxylate and sulfate FluoSpheres®, *N*-(biotinyl)-1,2-dihexadecanoyl-sn-glycero-3-phosphoethanolamine, *N*-(fluoresceinthiocaramoyl)-1,2-dihexadecanoyl-sn-glycero-3-phosphoethanolamine (FITC-PE), and FITC-conjugated neutralite avidin were obtained from Molecular Probes. Ascites containing Thy1 antibody was from Accurate Chemical, and the IgG fraction was obtained by purification on a DEAE affigel blue column. FITC-conjugated goat anti-mouse Fab fragments were from Cappel. For passive absorption to sulfate latex, avidin or Thy1 antibody was added to the spheres (0.1–0.5% solids) at concentrations ranging from 10–200 μg/ml in 0.1× phosphate buffered saline and allowed to attach for 2 hr. For covalent coupling of protein to carboxylate latex, the protein was added to FS in 15 m*M* 2-(*N*-Morpholino)ethanesulfonic acid buffer adjusted to pH 5.5 with dilute HCl. After 15 min at room temperature to allow the proteins to absorb to the FS surface, 1-ethyl-3-(3-dimethylaminopropyl)-carbodiimide was added to the mixture at a final concentration of 4 mg/ml. The activation of carboxylates and coupling to the protein via amide bond formation was allowed to proceed for 2 hr at room temperature. The reaction was terminated by the addition of either 0.1 M ethanolamine or 0.1 M glycine adjusted to pH 8.5. For both passively and covalently derivitized FS, unbound protein was removed by extensive dialysis in tubing with a 300,000 molecular weight cutoff. Just prior to use or assay, hydrophobic binding sites were blocked with 10 mg/ml BSA. Quantitation of avidin labeling was done on an aliquot of FS with [^{3}H]biotin (200 nM final, 60 Ci/mmol). Briefly, [^{3}H]biotin was added to the FS and allowed to incubate for 15 min at room temperature. Unbound radiolabel was removed by three successive cycles of centrifugation and resuspension in an epindorf centrifuge, and bound radiolabel was determined by liquid scintillation counting of the pelleted FS. Nonspecific binding was determined in the presence of a 100-fold molar excess on nonradioactive biotin. For the experiments described below, FS incorporating 8–20 biotin binding sites per FS were used for cell labeling.

Cell Labeling

For lipid labeling, a 200-fold stock solution of bPE in ethanol (1 mg/ml) was dispersed by sonication and diluted immediately into medium

A. The diluted solution was applied immediately to the cells at 4° C for 10 min and followed with three washes of medium A at 4° C. Immediately before use, labeled FS were blocked with 10 mg/ml BSA, sonicated in a bath sonicator to disperse aggregates, diluted into medium A and filtered through a 0.2 μm syringe filter to remove most dimers and any aggregates persisting after sonication. For FS labeling, particle concentrations were in the 10 pM range, but the dilution was empirically determined before each use to provide cells that were labeled so that most cells had several FS, but not so densely labeled that tracking of individual particles would be complicated by neighboring particles. Incubation with dispersed FS was for 5 min at room temperature, followed by three washes with medium A.

Microscopy

Video microscopy was performed on a Zeiss Axiovert 35 inverted microscope using a 100× 1.3 NA plan-achromat objective. A Hamamatsu C2400 with a SIT camera tube is connected to one port via a Zeiss 4× adapter, a Photometrics cooled charge coupled device (CCD) camera is mounted directly onto another port, and a Hamamatsu intensified interline transfer CCD camera to a third port with and without the 4× adapter. Both 100 W Hg and 75 W Xe excitation sources were examined in this study for epifluorescence illumination. Chambers containing the cells were maintained on the microscope stage in a humidified environment under a constant stream of 5% CO2/95% air in a heated stage compartment capable of maintaining temperatures from ambient to 40° C ± 1° C. Omega excitation (540DF23 or 560DF40), dichroics (565DRLP or 595DRLP) and emission filters (590DF35 or 635DF28) were used.

Cells with FS were selected by simultaneously viewing with both phase and fluorescence optics through the oculars. After extinguishing the phase source, selecting the SIT camera port, and focusing on the FS, the camera gain, offset and sensitivity were adjusted to maximize the signal to noise for monomeric FS (S/N) while minimizing the number of saturated pixels in the FS image, the camera lag, and blooming of the FS image. The few FS remaining in solution after washing did not remain in focus for the duration of an experiment and were readily distinguishable from FS attached to the cell surface. Full-frame images were captured for 4 sec and digitized into a 640 × 480 memory plane with 8 bits of grey-scale intensity at video rates using NIH-Image software for data acquisition and either Perceptics PixelBuffer and PixelStore or a Scion LG-3 with 64 MB of onboard memory NuBus digitizer cards incorporated into a Macintosh IIx computer. After capturing sequences, individual images were viewed at 4 frames/sec, and, if usable, transferred for storage in digital format to an Access International gigabyte optical disk. Nonusable sequences included those whose images contained too many saturated pixels, had insufficient S/N, or had FS that did not remain in the field of view for the duration of the experiment.

Image Analysis

For SPT, FS centroids from sequential images were obtained using NIH-Image (v. 1.52) and custom written HyperCard software for the Macintosh. Briefly, using NIH-Image, images were retrieved, pixel aspect ratios corrected, convolved with a 5 × 5 Gaussian kernel, look up tables were inverted and a 30 × 30 array of pixel intensities were extracted around each FS in each image in the sequence and saved as a text file. Using custom written HyperCard software for the Macintosh which was written to perform similarly to C code kindly provided by R. Sterba and M. Sheetz, an intensity weighted centroid was calculated (Gelles et al., 1986; Schnapp et al., 1988) from the intensity values in each text file for all intensities above an interactively-defined threshold that was dependent upon the background intensity. From the centroids for each FS, MSD values and statistical standard deviations dependent upon the number of observations were calculated using Eqs. 1 and 2 (Gross & Webb, 1988; Qian et al., 1991):

$$MSD(n\delta t) = (N-1-n)\sum_{j=1}^{N-1-n}\{[x(j\delta t + n\delta t) - x(j\delta t)]^2 + [y(j\delta t + n\delta t) - y(j\delta t)]^2\} \quad (1)$$

$$\rho(t) = 4Dn\delta t\sqrt{(2n+1)/3n(N-n+1)}, \quad (2)$$

where MSD is the mean square displacement, N the total number of independent determinations of the centroid position, n the interval number, δt the time between observations, $[x(j\delta t), y(j\delta t)]$ to centroid position at $j = n$, $[x(j\delta t + n\delta t), y(j\delta t + n\delta t)]$ the centroid position at $j = n + 1$, $\rho(t)$ the statistical deviation at time interval t, and D the diffusion coefficient. Theoretical MSD for unrestricted diffusion were calculated using Eq. 3:

$$MSD = 4Dn\delta t \quad (3)$$

Relative deviations from MSD values were calculated as described (Kusumi et al., 1993) using Eq. 4:

$$RD(N,n) = MSD(N,n)/4D_{2\text{–}4}n\delta t, \quad (4)$$

where $RD(N,n)$ is the ratio of the MSD at interval n from the MSD predicted using the initial diffusion coefficient, $D_{2\text{–}4}$, obtained from the least squares fit of the MSD data from the second, third and fourth time interval. The RD_{min} and RD_{max} values for the simulated data for unrestricted diffusion were determined to include a 95% chance for finding the particles as described by Kusumi et al. (1993). Graphics and linear regression analyses were performed in the spreadsheet applications Wingz (Informix Software, Lenexa, KS). For FS in some sequences, the S/N ratio was insufficient to accurately determine the centroid with the automated intensity threshold. In these instances, the threshold was determined interactively and then used for the centroid calculation. If this was required for more than six of the images in a given sequence (~5%), the sequence was classified as unusable. Some geometric distortion was introduced into our images, most likely due to the quality of the 4× adapter lens and the nature of signal enhancement in the SIT camera. However, distortion was extreme only near the image-edges, and FS near the edge were not examined by STP analyses.

Computer simulation of unrestricted and restricted diffusion in different domain sizes was done using custom written HyperCard software for the Macintosh. The distance of individual jumps was fixed and the direction allowed to vary randomly. In the case of restricted diffusion, tracers began in a randomly chosen location within the domain, and collisions with the barrier walls were elastic.

Results

Fluorescence Nanovid Microscopy: Technical Considerations

The choice of camera is essential for real-time particle tracking. The advantages of three cameras were exam-

ined in the present study, including a Photometrics cooled slow scan CCD camera, an intensified Hamamatsu interline transfer CCD camera, and a Hamamatsu SIT camera. The slow scan CCD camera, while providing the greatest sensitivity and having the largest dynamic range, is limited to studying slowly diffusing particles (Gross & Webb, 1988; Anderson et al., 1992) because obtaining images with sufficient S/N requires integration of the signal and because full frame readout and storage times requires many seconds. The use of CCD cameras with large pixel arrays that are currently available (i.e., 2000 × 2000) that allow on frame transfer under software control could be useful (Lasser-Ross et al., 1991), but the large pixel size which is best for fluorescent imaging (i.e., ~23 μm^2) makes the cost of such cameras prohibitive. The intensified CCD and SIT cameras have comparable sensitivities. The principle advantage of the intensified CCD is the near absence of persistence of signal, or lag, at the same incident light intensity when compared to the SIT camera. However, while FS imaged with the intensified CCD can be accurately tracked at lower magnifications (Fein et al., 1993), at the magnifications used in this study, individual images from the intensified CCD had insufficient S/N even at maximum intensifier gain for accurate centroid determination and were complicated by the "noise" introduced into the imaged FS by intensifier photon statistics. The S/N can be improved and photon statistical noise eliminated by averaging several frames, but this occurs with a sacrifice in temporal resolution and, when particles are moving rapidly, a corresponding loss of spatial precision. There is also considerable geometric distortion introduced into the image when using the intensifier and, for particles with significant movements, accurate particle tracking would require geometric decalibration of the images prior to single particle tracking (Jeričevič et al., 1989). The high resolution vidicon tubes often used for nanovid microscopy of colloidal gold can show significant lag even at relatively high incident light and limit tracking accuracy of rapidly moving particles. The SIT cameras are noted for lower lag when compared to vidicon cameras, but this is highly dependent upon the incident light level (Inoué, 1989). Although the camera sensitivity (the voltage across the photocathode and the silicon target) was always minimized in these experiments, the third field lag was tested in images of stationary FS to determine the minimum size of FS that could be used for accurate particle tracking. For a 100 nm FS, the mean intensity of the pixels encompassing the FS in the third field after removal of excitation was only about 12–18% of the original mean value, thus the camera lag was not too excessive and is actually slightly superior to that seen in the vidicons when imaging colloidal gold at higher incident light (*data not shown*). Smaller FS (30 nm) required increasing the SIT camera tube sensitivity to near maximum values, and while this provides images with sufficient S/N for STP, it resulted in substantial lag (>35%) and could not be used for accurately tracking rapidly diffusing particles at the magnification used in this study.

In SPT, tracking precision is determined not only by pixel size, and thus magnification, but also by image S/N (Schnapp et al., 1988). To determine the maximum spatial accuracy for SPT with our system, stationary 100 nm FS were imaged for 4 sec under the conditions to be used for the experiments. The intensity-weighted centroids were determined from the pixels with intensities above a user-defined threshold (for example, the black contour band in Fig. 3*B*) and are shown in Fig. 1. Presumably the FS did not move and all centroids should be at the origin. For a 4 sec-sequence of 120 images of fixed FS, the mean distance of the centroids from the origin is 7.5 ± 0.4 nm and is due to camera distortions, stage movements due to vibrations, and other sources of instability. The maximum distance of any of the FS centroids from the origin was 16 nm. Imaging multiple FS simultaneously and correcting the movements to an arbitrarily defined origin did not produce more accurate results (*data not shown*). As the velocity of the FS increases, movements can induce tailing and other nonGaussian intensity distortions into the image and reduce S/N, thereby reducing the tracking precision. However, most FS on the cell surfaces with D_c values in the range of 10^{-9} cm^2/sec or lower do not suffer deleteriously from this phenomenon.

Lipid Mobility by Fluorescence Nanovid Microscopy

Figure 2 shows images of fibroblasts that are labeled with avidin FS. These images were obtained using the slow scan CCD camera by simultaneously illuminating with sources for transmitted light using phase optics to identify cell boundaries and fluorescence optics to identify the FS. The cells in Fig. 2*A* were prelabeled with bPE and represent specific binding, and the cells in Fig. 2*B* were not prelabeled with bPE and represent the amount of nonspecific binding. In Fig. 2*C*, a cell was likewise imaged with the SIT camera, but at the higher magnification used for SPT. In all three figures, the nucleus, nuclear membrane, nucleolus and other intracellular organelles can be seen. In both images, some FS not in the focal plane can be seen by adjusting the focus from the top to bottom surface, but there are many more FS bound to the cells prelabeled with bPE. Despite steps to limit aggregation, some aggregates either persist or form after labeling (large arrow in Fig. 2*A,C*), but for SPT only individual FS were followed (small arrows in Fig. 2*A,C*), and these are easily distinguished by intensity profiles. Many of the negatively charged FS attach to the substratum due to the presence of the poly-D-lysine mixture used to coat the glass cover slip to promote cell adhesion

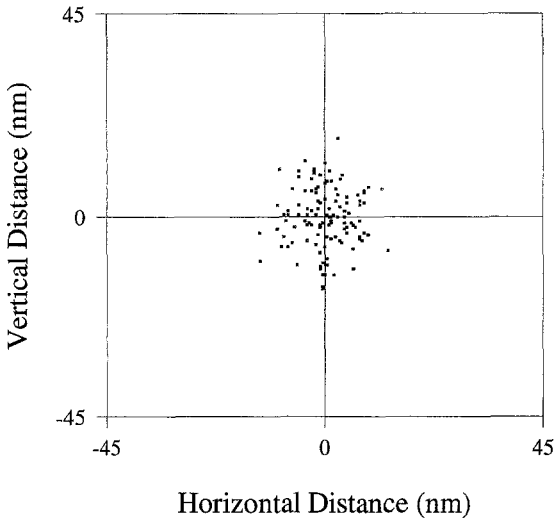

Fig. 1. Maximum tracking precision using FNM and SPT. The centroids from a stationary 100 nm FS obtained from analysis of images obtained over a 4 sec interval by "on-the-fly" digitization of the output from a SIT video camera are shown. The centroids, calculated for a FS that contained about 80 pixels with intensities significantly greater than background (*see* for example Fig. 3*B*) are all confined to a region smaller than 1 pixel (at the magnification used pixel have dimensions of about 45 nm × 45 nm). The mean distance of the centroids from the origin is 7.5 ± 0.4 nm. In theory, the centroids from all of the images should be at the origin, the scatter is due to variations in position due to the imaging system including camera noise and vibrations affecting the microscope stage.

and due to the fact that much of the bPE adheres to this surface (determined using FITC-conjugated avidin or using FITC-PE by itself, *data not shown*).

Fibroblasts were labeled with bPE followed by FS that had been derivitized with neutralite avidin. As in other mobility studies, cross-linking can lead to depressed values for D_c, so it is desirable to use paucivalent probes and preferable to use monovalent probes. However, it was shown previously that using paucivalent probes severely depresses surface labeling and causes only about a twofold difference in the D_c measured (Lee, Ishihara & Jacobson; 1991). In light of these constraints, a practical balance was struck, and the results below were obtained with FS labeled with approximately 8–20 biotin binding sites per FS, as assayed by the ability to precipitate [^{3}H]biotin (*data not shown*). In many preparations, a fraction of the FS showed little mobility ($D_c < 10^{-12}$ cm^2/sec) and these FS were excluded from the mean because they could not be extracted by Triton-X100, and they demonstrated a stationary mode of diffusion which differed from the majority of the particles. Addition of Triton-X100 to the medium did release all of the rapidly mobile FS from the membrane suggesting that they are bound to detergent soluble lipids (not shown).

Figure 3 shows representative results for diffusion of avidin FS on the surface of a bPE labeled fibroblast. In Fig. 3*A*, a 128 × 128 pixel region of interest from one 4 sec sequence of two diffusing avidin-labeled FS on bPE-labeled fibroblasts are shown at 0.5 sec-intervals. Figure 3*B* is a surface plot of a 50 × 50 array of pixel intensities encompassing the two FS from the 3.5 sec-time point in Fig. 3*A*. The intensity distributions in the spots are roughly Gaussian in shape. In calculating the centroid, only the pixels with intensities significantly above background were used. The complete paths traced by the FS centroids over the 4 sec are shown in Fig. 3*C*. The general accuracy of the tracking technique is demonstrated here as the calculated paths correspond precisely to the movements seen in Fig. 3*A* and to the full video record. This was the case for every FS monitored by SPT. The movements, characteristic of Brownian motion, appear to be undirected and changes in direction occur frequently and abruptly. Individual 'steps' over the 33 msec-observation period (1 frame) range from less than 12 (our maximum precision) to more than 200 nm. Of the 36 FS included in this analysis, maximum displacement observed over a 4 sec-interval approached three microns. The plots of MSD vs. time interval for the same two FS shown in Fig. 3*A,C* are shown in Fig. 3*D*. The bold line represents the theoretical value that would be obtained for unconstrained diffusion in two dimensions with a D_c of 1×10^{-9} cm^2/sec.

A histogram of the D_c values determined from the initial one-half second of diffusion for 36 FS is shown in Fig. 4*A*. Only the initial portion of the individual MSD plots were used to calculate the individual D_c values because, for many FS the stochastic nature of diffusion resulted in significant deviations from theoretical displacements at longer time intervals. In Fig. 4*B*, the MSD vs. time interval plot for the ensemble average of all 36 beads is shown. The ensemble average D_c for bPE in the membrane region between the leading edge and the supernuclear region was $0.80 \pm 0.11 \times 10^{-9}$ cm^2/sec and is represented by the plotted points (Fig. 4*B*). The theoretical line lies well within the predicted standard deviation for the experimental curve, and the failure of this curve to deviate appreciably from the theoretical linear value indicates that neither constraints to diffusion nor membrane flow are actively occurring in these cells over the duration of the experiment. Barriers to lateral diffusion such as confinement to a small membrane domain would have appeared in the plot as a deflection of the curve toward the time axis (less than theoretical displacement at longer time intervals). Diffusion accompanied by membrane flow or movements with constant velocity would have appeared as a deflection toward the MSD axis (greater than theoretical displacement at longer time intervals) (Qian et al., 1991). That appreciable membrane flow was not occurring in these cells under the experimental conditions was confirmed by performing time-lapse video-FRAP of DiI recovery in DiI-labeled

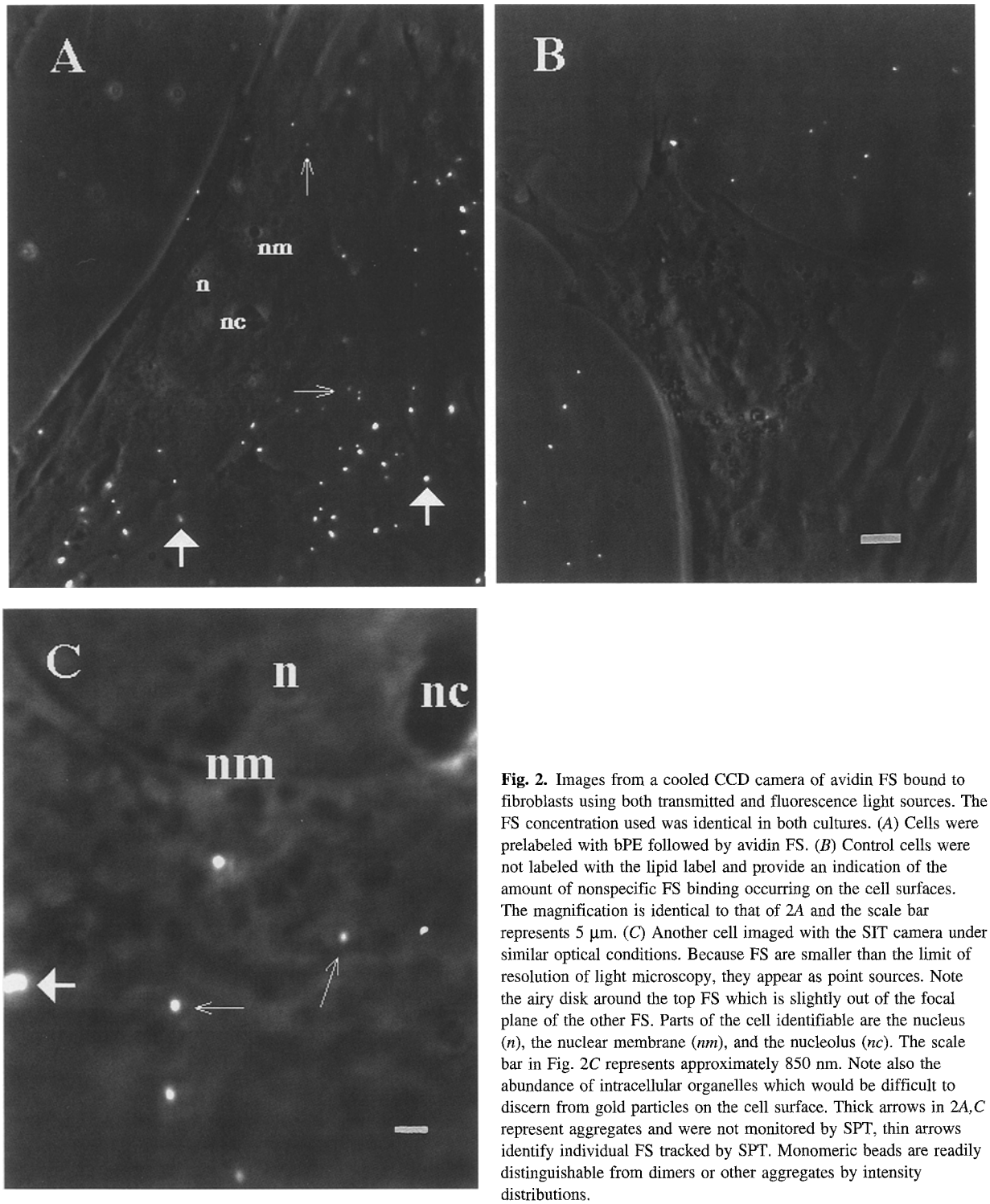

Fig. 2. Images from a cooled CCD camera of avidin FS bound to fibroblasts using both transmitted and fluorescence light sources. The FS concentration used was identical in both cultures. (*A*) Cells were prelabeled with bPE followed by avidin FS. (*B*) Control cells were not labeled with the lipid label and provide an indication of the amount of nonspecific FS binding occurring on the cell surfaces. The magnification is identical to that of 2*A* and the scale bar represents 5 μm. (*C*) Another cell imaged with the SIT camera under similar optical conditions. Because FS are smaller than the limit of resolution of light microscopy, they appear as point sources. Note the airy disk around the top FS which is slightly out of the focal plane of the other FS. Parts of the cell identifiable are the nucleus (*n*), the nuclear membrane (*nm*), and the nucleolus (*nc*). The scale bar in Fig. 2*C* represents approximately 850 nm. Note also the abundance of intracellular organelles which would be difficult to discern from gold particles on the cell surface. Thick arrows in 2*A,C* represent aggregates and were not monitored by SPT, thin arrows identify individual FS tracked by SPT. Monomeric beads are readily distinguishable from dimers or other aggregates by intensity distributions.

cells, and Thy1 recovery on cells labeled with anti-Thy1 and FITC-conjugated goat anti-mouse Fab fragments (*data not shown*). Cell migration was not significant under our experimental conditions as assessed by SPT of nucleoli and movements of the leading edge, and no correction for cell migration was included.

Protein Mobility by Fluorescence Nanovid Microscopy

To examine the mobility of protein in the plasmalemma, FS modified with monoclonal antibodies directed against the Thy1 antigen were prepared. The Thy1 antigen is a

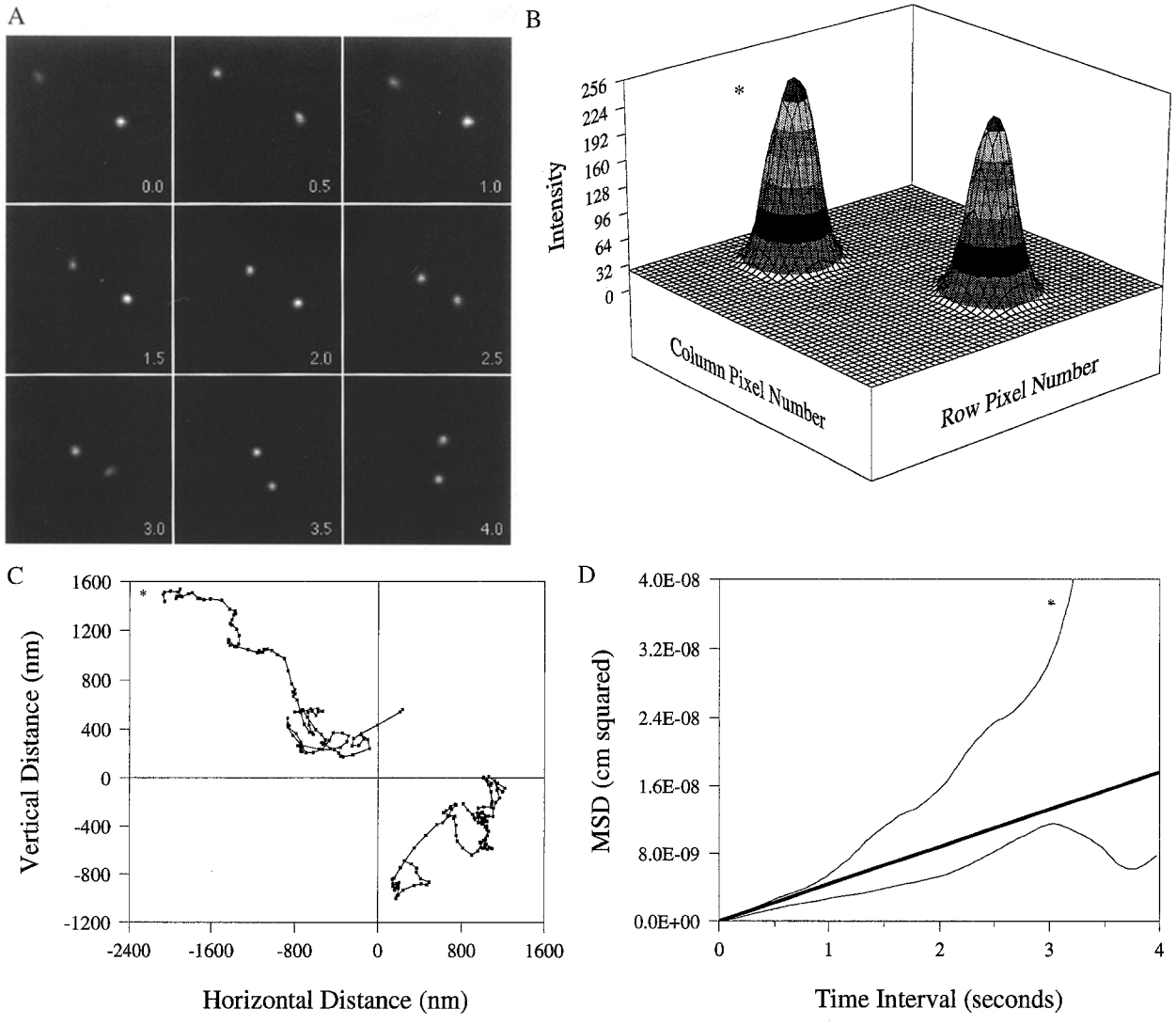

Fig. 3. Single particle tracking of lipids labeled with FS on the surface of one fibroblast. (*A*) Regions of interest taken from images in a 4 sec-sequence showing movements of two avidin-labeled FS on the surface of a bPE labeled fibroblast. The images shown were taken at 0.5 sec-intervals, and are 128 × 128 pixels, or about 5.7 μm on each side. The leftmost FS is identified with an asterisk in this figure and in the following graphs derived from these data. (*B*) Surface plots for the beads at the 3.5 sec-interval shown in Fig. 3*A* showing intensity as a function of pixel coordinate. The imaged beads give intensity profiles which are roughly Gaussian in shape. In calculation of the centroids, only those pixels with intensities above a user-defined threshold are included in the centroid calculation (for example, pixels with intensities within and above the black contour band). (*C*) The complete paths traced by the two particles shown in Fig. 3*A* over the entire 4 sec-interval (120 data points for each bead). Comparing Fig. 3*C* with Fig. 3*A* demonstrates the accuracy of the tracking methodology as the paths obtained from the centroids agree identically with the observed bead movements from the video images. Individual movements are Brownian in nature and, if barriers to lipid diffusion are present, they must allow for domains with diameters approaching 3 microns, the maximum unobstructed distance observed under the experimental conditions. (*D*) Diffusion coefficients can be obtained from the ensemble averaged MSD versus time interval plots. The thin lines correspond to the two FS in Fig.3*A–C*, and the bold line represents the theoretical values for unconstrained diffusion in two dimensions with a diffusion coefficient of 1×10^{-9} cm^2/sec.

29 kD protein that is linked to the extracellular leaflet of the plasmalemma via a GPI anchor. This protein, a member of the immunoglobin superfamily, is present on fibroblasts, neurons, and thymocytes. Analyzing paths traced by 54 different FS indicated the presence of two different populations based on D_c. Several different path types were observed for the diffusing Thy1 FS. Figure 5*A* shows the path traced by a Thy1 FS that can be classified as exhibiting the stationary mode of diffusion as defined by Kusumi et al. (1993). The movements near the origin are near the limit of our precision and cannot be considered to accurately depict the path. However, toward the end of this observation period (at about 3.5 sec) the FS underwent a significant displacement. In Fig. 5*B*, a Thy1 FS is shown that could be restricted to a domain within which unrestricted diffusion can occur.

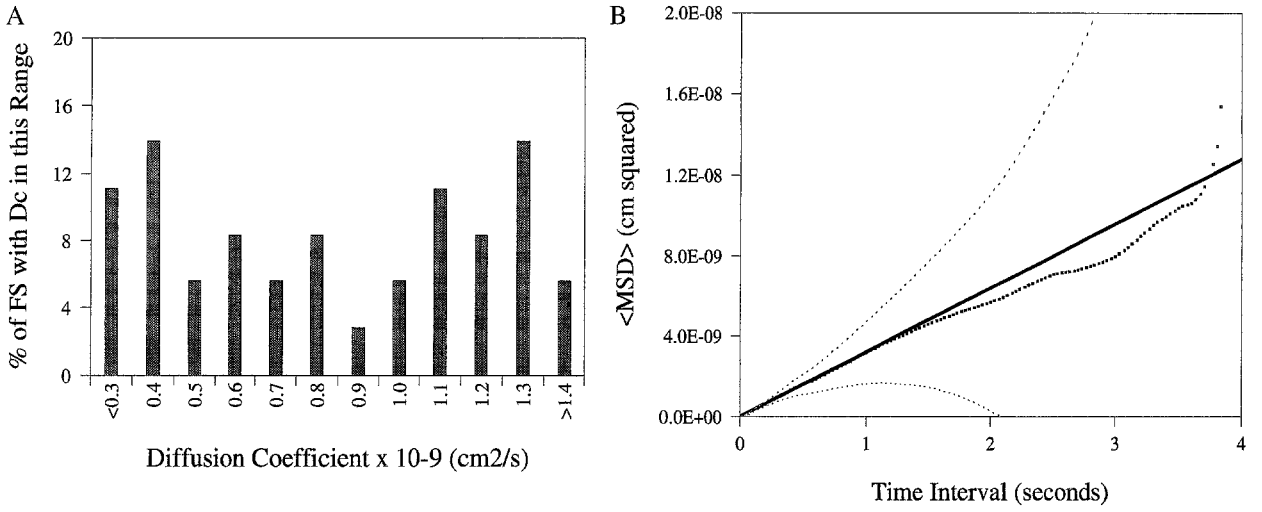

Fig. 4. Diffusion coefficients of lipid FS on the surface of fibroblasts. (*A*) Histogram of diffusion coefficients obtained for all 36 FS in the rapidly moving population ($D > 1 \times 10^{-12}$ cm^2/sec). The maximum D_c calculated was 2.2×10^{-9} cm^2/sec. Because net displacements for some FS are small, leading to plots which tend to bend toward the time interval axis, diffusion coefficients were calculated from the first one-half second of diffusion, where this effect was reduced. (*B*) Ensemble average MSD *vs.* time interval for all 36 FS. The bold line represents the theoretical value for unconstrained diffusion in two dimensions with a diffusion coefficient of 0.80×10^{-9} cm^2/sec, the value determined by linear regression from the data for all FS. The theoretical curve lies well within the range of statistical standard deviation (broken lines) for the experimental MSD curve with 120 independent observations.

In Figure 6*A*, a histogram of the D_c values calculated from the first one-third second of Thy1 diffusion is shown. Based on the D_c two broad populations were identified. Sixty-one percent of the FS had a mean D_c of $6.1 \pm 1.1 \times 10^{-10}$ cm^2/sec (4 FS had D > 10^{-9} cm^2/sec), while 39% had a mean D_c of $5.7 \pm 1.5 \times 10^{-12}$ cm^2/sec. Representative plots of MSD vs. time interval for nine of the Thy1 FS in the rapidly moving population are shown in Fig. 6*B*. The ensemble average MSD for all of the rapidly moving FS is shown (Fig. 6*C*) with corresponding theoretical statistical standard deviations (Qian et al., 1991). That the majority of most of the individual FS MSD paths fall within the standard deviation from the mean, that there is no overlap of the standard deviation with the theoretical value for unconstrained diffusion (except at very long time intervals), and that there is significant departure of the ensemble average curve from the theoretical values of unconstrained diffusion are indicative of restricted diffusion.

Proving confinement of individual FS to domains by SPT is not possible because the stochastic nature of diffusion will result in many paths that show little displacement even when no constraints are present (Kusumi et al., 1993; Saxton, 1993). While the deviation of the Thy1 ensemble MSD plots suggest restricted diffusion, to provide further support for this conclusion, we performed the analyses of Kusumi et al. (1993) on the rapidly moving Thy1 population. This involves simulating unrestricted diffusion and determining the relative deviation (RD) of the MSD from the expected values predicted from the initial diffusion coefficient (D_{2-4}) as a function of the number of observations (N, 120 in our case) and the observation time interval ($n\delta t$) (Eq. 3 in Materials and Methods). More than 250 simulations of unrestricted diffusion were performed, and the histograms of RD as a function of time interval are shown in Fig. 7*A*. These histograms can be useful for inferring nonisotropic diffusion demonstrated by groups of particles. From the RD histograms for the simulated data for unrestricted diffusion, values of RD_{min} and RD_{max} (the RD values between which there exists a 95% probability of finding a particle with unrestricted diffusion) can be determined.

To compare the results for the rapidly moving Thy1 FS to what is expected for molecules undergoing restricted diffusion, diffusion was modeled in square domains with "fences" that were either 400, 600, 800 or 1000 nm long. Within the domain, the tracers diffused freely with a D_c of 6.1×10^{-10} cm^2/sec for 120 steps, and they rebound from barriers with elastic collisions. In the upper part of Fig. 7*B* the representative paths of centroids in each of the domains of different size is shown, and in the lower part of Fig. 7*B* the corresponding ensemble MSD plots for 25 tracers are shown. In each of the lower plots, the thin line is the MSD plot for unconstrained diffusion. In accordance with our expectations, as the size of the domain decreases, the tracer spends more time sampling the domain boundaries and results in greater deflections of the MSD plot. While the histograms for unconfined diffusion can be useful for inferring nonisotropic diffusion, the level of the analysis is essentially the same as afforded by the MSD plots. For analyzing restricted diffusion plots of RD *vs.* n are more informative. The ensemble average RD *vs.* n data for the rapidly mov-

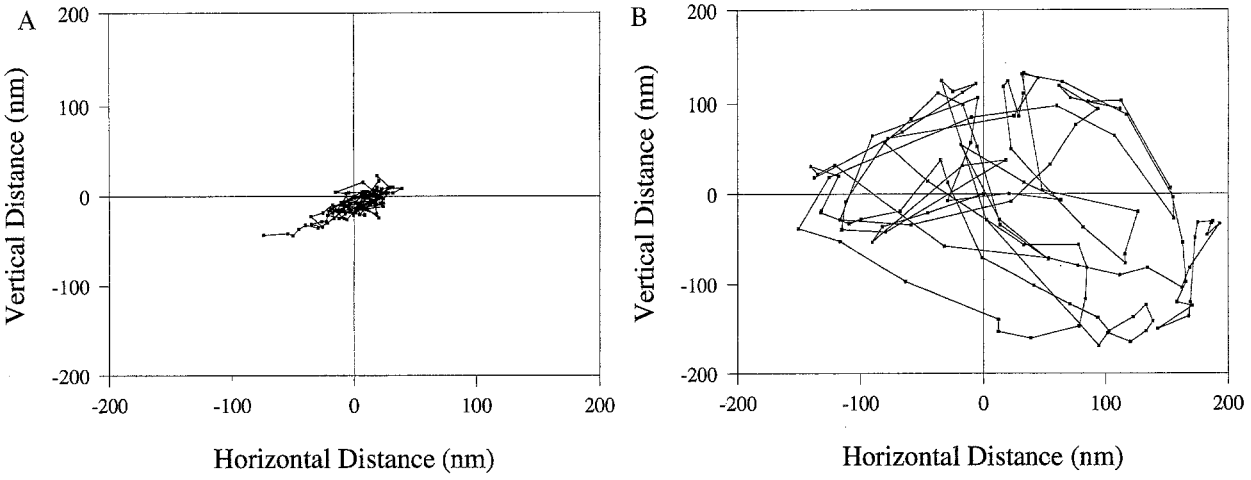

Fig. 5. Representative paths for two anti-Thy1 labeled FS on the surface of fibroblasts. (*A*) A FS that showed little net displacement over the 4 sec-interval. The majority of the points near the origin are at or near our tracking resolution, but the movements at the end of the sequence are significantly different. (*B*) A FS that apparently was capable of diffusion only within a restricted domain with a diameter of about 400 nm. No discernible structure was evident on the cell when viewed with phase or DIC optics.

ing Thy1 population and for the simulated restricted diffusion data are plotted in Fig. 7*C* along with the RD_{min} and RD_{max} determined for unrestricted diffusion. If the restricted diffusion results from direct anchoring to cytoskeletal or other laterally immobile components, the ensemble RD *vs.* n plots should be initially restricted, and remain so with increasing n (in fact, a plot of RD *vs.* n for the stationary FS shown in Fig. 1 is smaller than RD_{min} for all n, *data not shown*). If the constraints are due to "corrals" within which unrestricted diffusion occurs, this will be evident as a transition of the ensemble plot from unrestricted to restricted diffusion with increasing n. From a comparison of the interval at which the ensemble average RD passes from unrestricted to restricted diffusion to the interval at which the data for simulated restricted diffusion passes from unrestricted to restricted diffusion, an estimate of the length of the mean Thy1 domain can be obtained. Thus, from Fig. 7*C*, the mean length of the Thy1 domain is estimated to be about 700 nm. This value is consistent with the paths traced by many of the rapidly moving Thy1 FS although there was considerable deviation from the mean for individual FS. However, the observation that the values of microscopic diffusion coefficients, D_{2-4}, for the simulated data were dependent upon the domain size and uniformly lower than the known values used in the modeling indicates that refinements in this methodology will be required in the future, so that domain sizes may be more accurately defined.

Discussion

In order to examine the potential organization of the plasmalemma of living cells into submicron domains, a technique capable of monitoring membrane dynamics in the submicron range is required. The use of fluorescence microscopy in membrane dynamics has been largely restricted to ensemble techniques which fail to provide spatial information on the mode of diffusion. Excimer formation monitors only distances on the nanometer scale, postelectrophoresis monitors only large regions of the cell surface, while FRAP studies are typically larger than 1 μm^2. Few reports utilizing fluorescence microscopy have monitored diffusion of individual particles in cell membranes; low density lipoprotein and viral particles bound to receptors have been followed on fibroblasts (Gross & Webb, 1988; Anderson et al., 1992). These probes have limited potential and cannot be modified for tracking other membrane components. The factors most responsible for limiting fluorescent microscopy in analysis of individual membrane components are photobleaching, sensitivity, and versatility. These problems can be overcome by using modified FS to track individual membrane components by fluorescence microscopy (Hicks & Angelides, 1992, 1994*a,b;* Fein et al., 1993). Photobleaching is virtually nonexistent because the fluorophores are trapped inside the latex and only minimally accessible to molecular oxygen and other radicals in solution. Detection is increased because FS contain hundreds to thousands of fluorophores and are readily imaged (Fein et al., 1993; Hicks & Angelides, 1994*b*). In addition, FS are readily modified with antibodies or other ligands to monitor various membrane components (Fein et al., 1993; Hicks & Angelides, 1994*a,b*). For monitoring rapidly diffusing particles in real time by fluorescence microscopy with nanometer level precision, SIT cameras are superior to solid state cameras. Here we report the use of a SIT camera in tracking individual FS with nanometer scale precision to monitor the mobilities

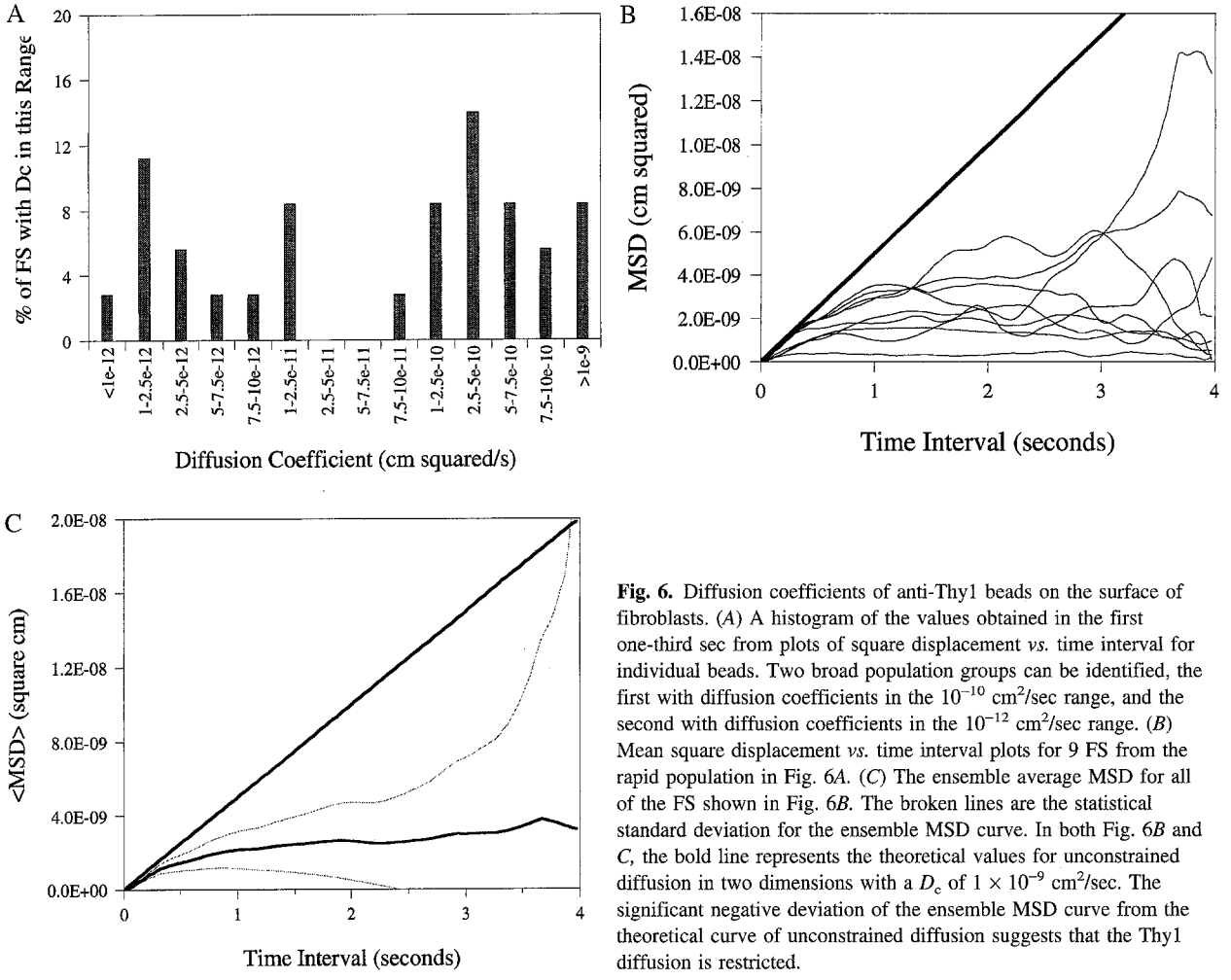

Fig. 6. Diffusion coefficients of anti-Thy1 beads on the surface of fibroblasts. (*A*) A histogram of the values obtained in the first one-third sec from plots of square displacement *vs.* time interval for individual beads. Two broad population groups can be identified, the first with diffusion coefficients in the 10^{-10} cm^2/sec range, and the second with diffusion coefficients in the 10^{-12} cm^2/sec range. (*B*) Mean square displacement *vs.* time interval plots for 9 FS from the rapid population in Fig. 6*A*. (*C*) The ensemble average MSD for all of the FS shown in Fig. 6*B*. The broken lines are the statistical standard deviation for the ensemble MSD curve. In both Fig. 6*B* and *C*, the bold line represents the theoretical values for unconstrained diffusion in two dimensions with a D_c of 1×10^{-9} cm^2/sec. The significant negative deviation of the ensemble MSD curve from the theoretical curve of unconstrained diffusion suggests that the Thy1 diffusion is restricted.

of lipid and Thy1 on the fibroblasts membrane by fluorescence microscopy.

Most of the information on the dynamic behavior of individual membrane components has come from nanovid microscopy monitoring colloidal gold or latex particles using intense incident light and brightfield or DIC optics (de Brabander et al., 1986, 1987, 1989; Geerts et al., 1987; Schnapp et al., 1988; Lee et al., 1993). Video enhanced contrast DIC microscopy (Allen et al., 1981) is used for detection of particles, and information is stored directly onto VHS tape or in other analog formats. A number of practical limitations are inherent in this methodology and can limit the region of the cell surface that can be monitored and the accuracy of the results. First, discriminating between intracellular organelles and gold particles is difficult, if not impossible, on some regions of the cell surface when using DIC optics (Sheetz & Elson, 1993). Second, storing images in analog formats and digitizing frames that are recalled with a frame grabber and time base corrector introduces distortion into the pixel intensities of the original image (Inoué, 1989). Third, high resolution cameras with vidicon tubes tend to show significant lag and reduce spatial precision in frame-by-frame tracking, even at relatively high levels of incident light (Inoué, 1989; Sheetz & Kuo, 1993). Fourth, intense illumination by a 100 W Hg arc lamp can induce cell damage upon prolonged exposure (Taylor & Salmon, 1989). Finally, the narrow focal range of small particles using DIC optics at high magnifications has limited most applications to the edges of relatively flat cells such as keratocytes and fibroblasts where high contrast images with sufficient S/N can be obtained (Sheetz & Elson, 1993). By exciting with a 75 W xenon arc through a 560 nm band pass filter and using epifluorescence microscopy, using real-time digitization of the video output from a SIT camera for a brief duration, and storing the images in digital format we have avoided the above-mentioned difficulties. Imaged FS have intensity profiles that are roughly Gaussian, and centroids from 100 nm FS can be accurately located with maximum precision on the order of 10 nm. Fluorescence microscopy also allows for the additional exciting possibility of simultaneously monitoring multiple membrane components.

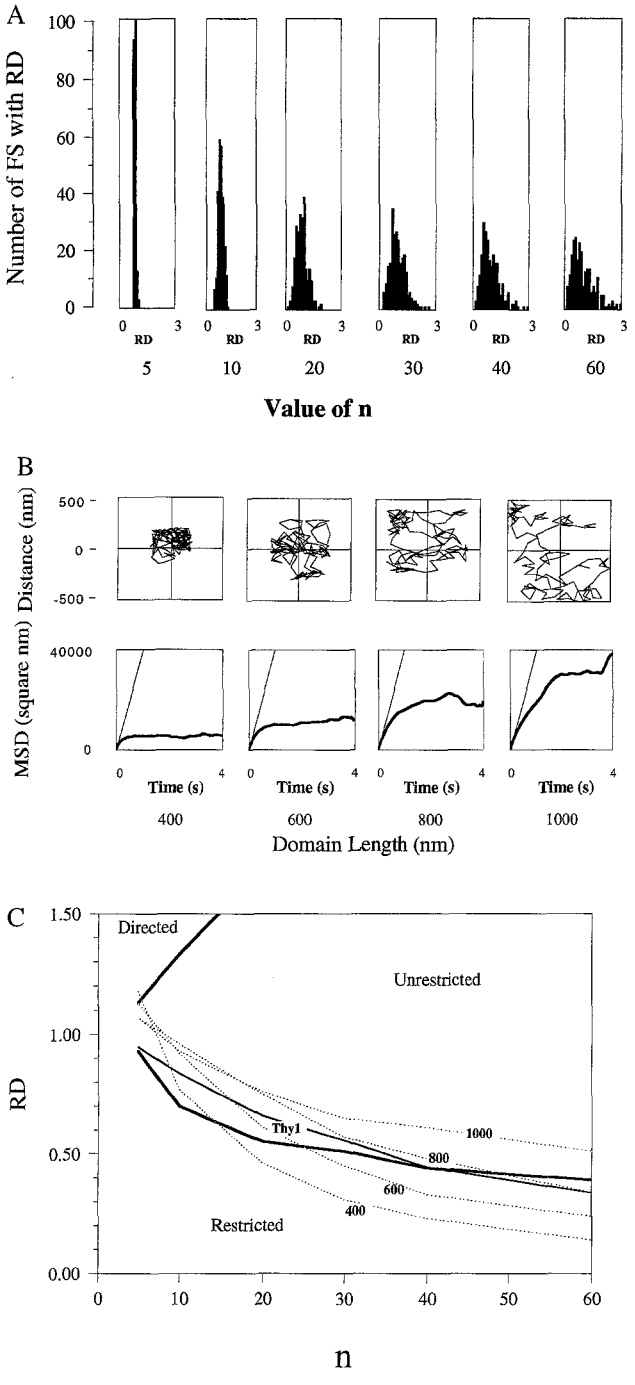

Fig. 7. Further analysis of the rapidly moving Thy1 FS. (*A*) Plots of *RD vs.* n for simulated unconstrained diffusion for more than 250 tracers. As *n* increases for a single value of *N* (120), the histograms get more complex. (*B*) Simulations of constrained diffusion in square "corrals" with "fences" of different length ranging from 400 to 1000 nm. Upper figures show paths of tracer centroids about the origin. These are not accurate reflections of the tracer paths, because points resulting from collisions at the domain boundary are not shown. Lower figures show MSD *vs.* time interval plots (bold lines) for the ensemble average of 25 tracers. The thin line represents the MSD for unrestricted diffusion with a D_c of 6.1×10^{-10} cm^2/sec. (*C*) Plots of relative deviation (*RD*) *vs.* observation number (*n*) for simulated restricted diffusion and for the rapidly moving Thy1 FS. The bold lines represent the RD_{min} and RD_{max} taken from the simulations of unrestricted diffusion. There is a 95% chance that FS undergoing unrestricted diffusion will be present between these extremes. Particles with restricted diffusion will appear below RD_{min} and particles that demonstrated directed diffusion will appear above RD_{max}. The transition of the Thy1 plot from unrestricted to restricted diffusion at increasing n indicates that Thy1 is allowed to diffuse freely within the domain. From the point at which the Thy1 curve crosses the RD_{min} curve, it is estimated that Thy1 is restricted to domains with a mean length of about 700 nm.

The maximum onboard digitizer random access memory that was available limited us to capturing 120 video frames in 'real time.' At relatively small values of n (above about 30, see the histograms in Fig. 7*A*), there is too much deviation in the RD values to unambiguously identify the mode of diffusion or to accurately estimate the size of the Thy1 domains with only 120 independent measurements of the FS position. Recently available upgrades in software that allow selection of ROIs from full frames, and the availability of 32 megabyte SIMMs make it feasible to collect as many as 1024 8-bit images with a 256 × 256 memory plane at video rates, and will lead to a greater ability to convincingly show significant deviations of the experimental data from unrestricted diffusion. The longer observation times that these improvements will allow can lead to false classification of diffusion modes for particles trapped in "corrals" with transient "fences" (Kusumi et al., 1993). Improvements and price reductions in computer hardware and software that will undoubtedly become available in the near future will make purely digital data collection and storage, such as we have done here, the preferred method for nanovid and SPT.

Table 1 summarizes comparisons of diffusion coefficients obtained by FRAP, nanovid, and FNM. Nanovid microscopy can accurately monitor the Brownian diffusion of individual lipid particles in artificial bilayers using either 40 nm colloidal gold and brightfield optics or 30 nm FS and epifluorescence microscopy (Lee et al., 1991; Fein et al., 1993). Monitoring lateral diffusion of individual lipids in cellular membranes using brightfield nanovid to monitor colloidal gold conjugated to anti-FITC on the surface of cells labeled with FITC-PE (Lee et al., 1993) detected no barriers to diffusion. The fraction of rapidly moving particles had an average D_c of about $1\text{–}2 \times 10^{-9}$ cm^2/sec, which was dependent upon the cell type, the cellular region examined, and the influence of the pericellular matrix. The lipid D_c value measured in cell membranes using nanovid was notably about threefold lower than the value obtained by the same methodology in artificial bilayers. In the study by Lee et al. (1993), the plasmalemma above the organelle-rich regions of the cytoplasm were avoided because unambiguous identification of gold particles was not possible.

Table 1. Comparisons of diffusion coefficients for the rapid population by FRAP, nanovid and FNM ($\times 10^9$ cm^2/s)[a]

	Lipids		GPI-linked proteins	
	Bilayers	Cells	Bilayers	Cells
FRAP	40–90[b]	5.4–9.5[c]	NA	2.7[d]
Nanovid	2.6–7.3[e]	1.1–1.7[c]	NA	1.0[f]
FNM	2.6[g]	0.80	2.5–5.6[g]	0.61

[a] For FRAP this is the mobile fraction. For SPT, the value represents the rapidly moving population.
[b] Taken from Derzko and Jacobsen (1980).
[c] Taken from Lee et al., (1993).
[d] Taken from Zhang et al., (1991).
[e] Taken from Lee et al., (1991). The large range results from probe valency.
[f] Taken from de Brabander et al., (1991).
[g] Taken from Fein et al., (1993). The GPI-linked proteins examined in this study were not Thy1, and the analysis was not performed with nanometer level precision. However, this should not be consequential as diffusion in artificial bilayers is unrestricted.
NA not available

The D_c measured in this study, focusing attention to the cellular region between the lamella and the nucleus, was 0.80×10^{-9} cm^2/sec, and is in close agreement to the value reported using colloidal gold, but is likewise threefold lower than the value determined for lipids in artificial bilayers using fluorescence microscopy (Fein et al., 1993). The small differences observed in lipid diffusion in cell membranes between the present study and the study of Lee et al. (1993) could be due to differences in membrane composition and organization of the cell types examined (primary rat cells and mouse 3T3 cells), differences in membrane organization between the different areas of the cell surface (the leading edge and supernuclear regions *vs.* the region above the organelle-rich cytoplasm), differences in the size of the particles used as probes (30 nm *vs.* 100 nm), or differences in the modified head group (biotin versus fluorescein) used as a probe. The ability of some of the lipid-bound FS in the present study to move distances of nearly 3 μm is in agreement with a model of membrane structure that allows for long-range lateral diffusion of some membrane components (Edidin, Kuo & Sheetz, 1991; Edidin, 1992; Lee et al., 1993). In summary, FNM provides data comparable to that observed by nanovid with transmitted light optics, both of which produce D_c values above fivefold lower than the values observed by FRAP, and D_c obtained using nanovid and FNM in cell membranes are about fivefold lower than those obtained for comparable probes in artificial bilayers.

Multivalent particles caused a twofold decrease in the observed D_c when measuring lipid diffusion, and it was suggested that this was due to increased resistance as multiple contact sites caused the membrane to partially wrap around the particle (Lee et al., 1991). For SPT of proteins, crosslinking could have severe consequences on lateral mobility and may require univalent probes. Thy1 was chosen for this study because previous reports using spot-FRAP to compare lateral mobility of Thy1 using probes capable of crosslinking the antigen (intact anti-Thy1 IgG) and monovalent probes (Fab fragments of anti-Thy1) indicated that there was less than a twofold differences in the D_c, even though two roughly equal populations based on lateral mobility were detected (Zhang et al., 1991; Zhang et al., 1992). In this study, two roughly equal populations of Thy1, based on lateral mobility, also were detected. The source of the constraining force on a portion of the Thy1 population is unknown and may vary with cell type. Possibilities include interactions with a transmembrane protein tethered to the cytoskeleton, labeling protein that was recently delivered to the membrane in immobile clusters, interactions with a component in the extracellular matrix, or trapping of the GPI anchor in segregated lipid microdomains (He et al., 1991; Thomas & Samelson, 1992; Brown, 1992; Hannan et al., 1993). The presence of a peak in the Thy1 histogram at about 2.5×10^{-12} cm^2/sec makes it tempting to suggest that interactions of the slowly moving Thy1 population with proteins immobilized by the cytoskeleton may be occurring. E-cadhedrin, a protein known to bind to actin filaments (Hirano et al., 1987), shows a similar peak in D_c histograms (Kusumi et al., 1993). While confinement of Thy1 to small domains on the fibroblast surface appears to be at odds with previous reports demonstrating that GPI-linked proteins in laser traps can be dragged through the membrane for long distances (Edidin, Kuo & Sheetz, 1991), the force applied to the particles in that study resulted in a translational energy that is considerably greater than that possessed by an individual molecule under physiological conditions. Furthermore, the study of Zhang et al. (1991) on mobility of GPI-linked proteins suggests that the lipid anchor is less responsible for the lateral mobility than the nature of the extracellular domain, and differences in either the GPI-linked proteins examined, or the cell type, could explain the apparent discrepancies.

We have shown here that FMN can be used to study dynamics of individual membrane components on cell surfaces with nanometer level precision. The photostability of the fluorophore in the FS, the ease of detection and the ability to modify the FS with antibodies, toxins or other ligands of interest should make it possible to monitor diffusion of many individuals cell surface components. In practice however, this will be much more difficult for proteins than for lipids. The majority of proteins whose lateral mobilities have been measured by FRAP possess some fraction which is immobile (McCloskey & Poo, 1984), but little explanation has been provided to explain this observation (Zhang et al., 1993).

In monitoring protein diffusion by FMN or nanovid, multivalent probes could potentially crosslink members from the two populations depressing the lateral mobility of the rapid fraction and complicating interpretation of the data. Indeed, the presence of a small slowly mobile fraction of lipid FS, which we interpret as being nonspecifically bound to immobilized proteins, is probably also present in the Thy1 measurements, meaning the relative size of the slowly moving Thy1 population is overestimated. This makes analysis of the slowly moving population difficult. However, univalent probes result in a significant decrease in specific labeling and likewise complicate data interpretation in a particle-by-particle assay of diffusion. The use of avidin as a secondary probe is valuable because the particle valency can be easily and accurately determined prior to experimentation with radiolabeled biotin or by the ability to bind biotin modified proteins (Fein et al., 1993).

Finally, it should be remembered that because of the stochastic nature of diffusion, unambiguously proving restricted diffusion for individual particles is not possible (Saxton, 1993; Kusumi et al., 1993). The advantage of FNM and nanovid over other techniques for monitoring lateral mobility are the scale on which membrane organization can be examined, and the ability to directly extrapolate results from ensemble average data to individual membrane components to provide insight into biological mechanisms accounting for nonisotropic diffusion.

This work was supported by National Institutes of Health grant NS28072 and the MS Society. B. Hicks is an National Institutes of Health extramural postdoctoral fellow NS09196. The authors wish to thank Richard Rodriquez and Fidelma O'Leary for proofreading the manuscript.

References

Allen, R.D., Allen, N.S., Travis, J.L. 1981. Video enhanced contrast, differential interference (AVEC-DIC) microscopy: A new method capable of analyzing microtubule related motility in the reticulopodial network of Allogramia laticollaris. *Cell Motil.* **1:**291–299

Anderson, C.M., Georgiou, G.N., Morrison, I.E.G., Stevenson, G.V.W., Cherry, R.J. 1992. Tracking of cell surface receptors by fluorescence digital imaging microscopy using a charge-coupled device camera. *J. Cell Sci.* **101:**415–425

Black, J.A., Kocsis, J.D., Waxman, S.G. 1990. Ion channel organization in the myelinated fiber. *Trends in Neurosci.* **13:**48–54

Brown, D.A. 1992. Interactions between GPI-anchored proteins and membrane lipids. *Trends in Cell Biol.* **2:**338–343

de Brabander, M., Nuydens, R., Geuens, G., Moeremans, M., de Mey, J. 1986. The use of submicroscopic gold particles combined with video contrast enhancement as a simple molecular probe for the living cell. *Cell Motil. Cyto.* **6:**105–113

de Brabander, M., Geerts, H., Nuydens, R., Nuyens, R. 1989. Detection of gold probes with video-enhanced contrast microscopy: Nanovid microscopy. *Am. J. Anatomy* **185:**282–295

de Brabander, M., Nuydens, R., Ishihara, A., Holifield, B., Jacobson, K., Geerts, H. 1991. Lateral diffusion and retrograde movements of individual cell surface components on single motile cells observed with nanovid microscopy. *J. Cell Biol.* **112:**111–124

Derzko, Z., Jacobson, K. 1980. Comparative lateral diffusion of fluorescent lipid analogues in phospholipid multilayers. *Biochemistry* **19:**6050–6061

Edidin, M., Kuo, S.C., Sheetz, M. 1991. Lateral movements of membrane glycoproteins restricted by dynamic cytoplasmic barriers. *Science* **254:**1379–1382

Edidin, M. 1992. Patches, posts and fences: proteins and plasma membrane domains. *Trends in Cell Biol.* **2:**376–380

Eisinger, J., Flores, J., Peterson, W.P. 1986. A milling crowd model for local and long-range obstructed lateral diffusion-Mobility of excimeric probes in the membrane of intact erythrocytes. *Biophys. J.* **49:**987–1001

Fertuck, H.C., Salpeter, M.M. 1976. Quantitation of junctional and extrajunctional acetylcholine receptors by electron microscope autoradiography after ^{125}I-α-bungarotoxin binding at mouse neuromuscular junctions. *J. Cell Biol.* **69:**144–158

Fein, M., Unkeless, J., Chuang, F.Y.S., Sassaroli, M., da Costa, R., Vaananen, H., Eisinger, J. 1993. Lateral mobility of lipid analogues and GPI-anchored proteins in supported bilayers determined by fluorescent bead tracking. *J. Membrane Biol.* **135:**83–92

Forshcer, P., Lin, C.H., Thompson, C. 1992. Novel form of growth cone motility involving site-directed actin filament assembly. *Nature* **357:**515–518

Geerts, H., de Brabander, M., Nuydens, R., Geuens, S., Moeremans, M., Mey, J.D., Hollenbeck, P. 1987. Nanovid tracking: a new automatic method for the study of mobility in living cells based on colloidal gold and video microscopy. *Biophys. J.* **52:**775–782

Gelles, J., Schnapp, B.J., Sheetz, M.P. 1988. Tracking kinesin-driven movements with nanometre-scale precision. *Nature* **331:**450–453

Gross, D.J., Webb, W.W. 1988. Cell surface clustering and mobility of the liganded LDL receptor measured by digital video fluorescence microscopy. *In:* Spectroscopic Membrane Probes. L.M. Loew, editor. pp. 19–45. CRC, Boca Raton

Hannan, L.A., Lisanti, M.P., Rodriguiz-Boulan, E., Edidin, M. 1993. Correctly sorted molecules of a GPI-linked protein are clustered and immobile when they arrive at the surface of MDCK cells. *J. Cell Biol.* **120:**353–358

Haverstick, D.M., Glaser, M. 1988. Visualization of domain formation in the inner and outer leaflets of a phospholipid bilayer. *J. Cell Biol.* **106:**1885–1892

He, H.-T., Naquet, P., Caillol, D., Pierres, M. 1991. Thy1 supports adhesion of mouse thymocytes to thymic epithelial cells through a Ca2(+)-independent mechanism. *J. Exp. Med.* **173:**515–518

Hicks, B.W., Angelides, K.J. 1992. Mechanisms of distributing sodium channels in myelinated axons. *Soc. Neurosci. Abstr.* **18:**408

Hicks, B.W., Angelides, K.J. 1994*a*. Imaging ion channel dynamics in living neurons by fluorescence microscopy. *In:* Ion Channels of Excitable Cells, Methods in Neurosciences Vol 19. T. Narahasi, editor, pp. 320-339. Academic, San Diego

Hicks, B.W., Angelides, K.J. 1994*b*. Imaging plasmalemma dynamics by single particle tracking of derivitized fluorescent microspheres. *In:* Proceedings of the 52nd Annual Meeting of the Microscopy Society of America. G.W. Bailey and A.J. Garratt-Reed, editors. pp. 174–175. San Francisco Press, San Francisco

Hirano, S., Nose, A., Hatta, K., Kawakami, A., Takeichi, M. 1987. Calcium-dependent cell-cell adhesion molecules (cadhedrins): subclass specificities and possible involvement of actin bundles. *J. Cell Biol.* **105:**2501–2510

Inoué, S. 1989. Video Microscopy. S. Inoué, editor. pp. 219, Plenum, New York

Jeričevič, Z., Wiese, B., Bryan, J., Smith, L. 1989. Validation of an

imaging system. *In:* Methods in cell biology volume 30, part b. Fluorescence microscopy of living cells in culture. D.L. Taylor and Y.-L. Wang, editors. pp. 48-82. Academic, San Diego

Kucik, D., Elson, E.L., Sheetz, M.P. 1990. Cell migration does not produce membrane flow. *J. Cell Biol.* **111:**1617–1622

Kucik, D.F., Kuo, S.C., Elson, E.L. Sheetz, M.P. 1991. Preferential attachment of membrane glycoproteins to the cytoskeleton at the leading edge of lamella. *J. Cell Biol.* **114:**1029–1036

Kusumi, A., Sako, Y., Yamamoto, M. 1993. Confined lateral diffusion of membrane receptors as studied by single particle tracking (Nanovid Microscopy). Effects of calcium-induced differentiation in cultured epithelial cells. *Biophysical J.* **65:**2021–2040

Lasser-Ross, N., Miyakawa, H., Lef-Ram, V., Young, S.R., Ross, W.N. 1991. High time resolution fluorescence imaging with a CCD camera. *J. Neurosci. Methods* **36:**253–261

Lee, G.M., Ishihara, A., Jacobson, K.A. 1991. Direct observation of Brownian motion of lipids in a membrane. *Proc. Natl. Acad. Sci. USA* **88:**6274–6278

Lee, G.M., Zhang, F., Ishihara, A., McNeil, C.L. Jacobson, K.A. 1993. Unconfined lateral diffusion and an estimate of pericellular matrix viscosity revealed by measuring the mobility of gold-tagged lipids. *J. Cell Biol.* **120:**25–35

Lupa, M.T., Caldwell, J.H. 1991. Effect of agrin on the distribution of acetylcholine receptors and sodium channels on adult skeletal muscle fibres in culture. *J. Cell Biol.* **115:**765–778

McCloskey, M., Poo, M.-M. 1984. Protein diffusion in cell membranes: some biological implications. *Int. Rev. Cytol.* **87:**19–81

Owicki, J.C., McConnell, H.M. 1980. Lateral diffusion in inhomogeneous membranes. Model membranes containing cholesterol. *Biophys. J.* **30:**383–392

Poo, M.-M. 1981. In situ electrophoresis of membrane components. *Annu. Rev. Biophys. Bioenerg.* **10:**245–276

Qian, H., Sheetz, M.P., Elson, E.L. 1991. Single particle tracking. *Biophys. J.* **60:**910–921

Rogers, W., Glaser, M. 1991. Characterization of lipid domains in erythrocyte membranes. *Proc. Natl. Acad. Sci. USA* **88:**1364–1368

Rubenstein, J.R.L., Smith, B.A., McConnell, H.M. 1979. Lateral diffusion in binary mixtures of cholesterol and phosphatidylcholines. *Proc. Natl. Acad. Sci. USA* **76:**15–18

Sako, Y., Kusumi, A. 1994. Compartmentalized structure of the plasma membrane for receptor movements as revealed by a nanometer-level motion analysis. *J. Cell Biol.* **125:**1251–1264

Saxton, J.M. 1987. Lateral diffusion in an archipelago. The effect of mobile obstacles. *Biophys. J.* **52:**989–997

Saxton, M.J. 1993. Lateral diffusion in an archipelago. Single particle diffusion. *Biophysical J.* **64:**1766–1780

Schmidt, C.E., Horwitz, A.F., Lauffenburger, D.A., Sheetz, M.P. 1993. Integrin-cytoskeleton interactions in migrating fibroblasts are dynamic, asymetric and regulated. *J. Cell Biol.* **123:**977–991

Schnapp, B.J., Gelles, J., Sheetz, M.P. 1988. Nanometer-scale measurements using video light microscopy. *Cell Motil. Cyto.* **10:**47–53

Sheetz, M.P., Kuo, S.C. 1993. Tracking nanometer movements of single motor molecules. *In:* Motility Assays for Motor Proteins, Methods in Cell Biology Vol. 39. J.M. Scholey, editor, pp. 134. Academic, San Diego

Sheetz, M.P., Turney, S., Qian, H., Elson, E.L. 1989. Nanometre-level analysis demonstrates that lipid flow does not drive membrane glycoprotein movements. *Nature* **340:**284–288

Sheetz, M.P., Elson, E.L. 1993. Measurement of membrane glycoprotein movement by single-particle tracking. *In:* Optical Microscopy, Engineering Methods and Applications. B. Herman and J.J. Lemasters, editors. pp. 285–294. Academic, San Diego.

Taylor, D.L., Salmon, E.D. 1989. Basic fluorescence microscopy. *In:* Fluorescence Microscopy of Living Cells in Culture. L. Wilson, editor, pp. 207–237. Academic, San Diego

Thomas, P.M., Samelson, L.E. 1992. The glycophosphatidylinositol-anchored Thy1 molecule interacts with the p60fyn protein tyrosine kinase in T cells. *J. Biol. Chem.* **267:**12317–12322

Yechiel, E., Edidin, M. 1987. Micrometer-scale domains in fibroblast plasma membranes. *J. Cell Biol.* **105:**755–760

Zhang, F., Crise, B., Su, B., Hou, Y., Rose, J.K., Bothwell, A., Jacobson, K. 1991. Lateral diffusion of membrane-spanning and glycosylphosphatidylinositol-linked proteins: toward establishing rules governing the lateral mobility of membrane proteins. *J. Cell Biol.* **115:**75–84

Zhang, F., Schmidt, W.G., Hou, Y., Williams, A.F., Jacobson, K. 1992. Spontaneous incorporation of the glycosyl-phosphatidylinositol-linked protein Thy1 into cell membranes. *Proc. Natl. Acad. Sci. USA* **89:**5231–5235

Zhang, F., Lee, G.M., Jacobsen, K. 1993. Protein lateral mobility as a reflection of membrane microstructure. *BioEssays* **15:**579–588